Geomorphology 408 (2022) 108247

Contents lists available at ScienceDirect

Geomorphology

journal homepage: www.journals.elsevier.com/geomorphology

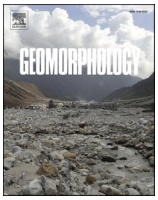

Episodic movement of a submarine landslide complex driven by dynamic loading during earthquakes

J.M. Carey [a,*], J.J. Mountjoy [b], G.J. Crutchley [c], D.N. Petley [d], C.F. Holden [e], Y. Kaneko [f], K. Huhn [g]

[a] GNS Science, 1 Fairway Drive Avalon, PO Box 30368, Lower Hutt, New Zealand
[b] National Institute of Water and Atmospheric Research, PO Box 14901, Wellington, New Zealand
[c] GEOMAR Helmholtz Centre for Ocean Research, Kiel, Germany
[d] Department of Geography, University of Sheffield, Sheffield S10 2TN, UK
[e] SeismoCity Ltd, Wellington, New Zealand
[f] Department of Geophysics, Kyoto University, Japan
[g] Centre for Marine Environmental Sciences (MARUM), University of Bremen, Bremen, Germany

ARTICLE INFO

Keywords:
Submarine landslides
Movement mechanisms
Earthquakes

ABSTRACT

Although subaqueous slopes on active continental margins are subject to a variety of failure styles, their movement mechanisms during earthquakes remain poorly constrained. A primary explanation is that few submarine landslides have been directly sampled for detailed investigation. We have conducted a series of dynamic shear experiments on samples recovered from the base of the Tuaheni Landslide Complex, located off the east coast of the North Island of New Zealand, to explore its behaviour during earthquakes. Our experiments suggest that whilst the basal landslide sediments can be prone to liquefaction in certain conditions, this is not a likely failure mechanism at the stress states operating in the low angled shear zone at the base of this landslide system. Instead, episodic landslide movement can occur through basal sliding when pore water pressures increase sufficiently to lower the shear zone effective stress to the material failure envelope. These low effective stress conditions are most likely to be reached during earthquakes that produce large amplitude, long duration ground shaking. The observed behaviour provides a credible mechanism through which subaqueous landslides moving on low angled shear zones in similar materials may be subject to episodic movement during earthquakes without undergoing catastrophic failure.

1. Introduction

Submarine landslides have long been recognized to initiate on low angled slopes on both active and passive continental margins (Prior and Coleman, 1978; Field et al., 1982; Hampton et al., 1996; Hühnerbach and Masson, 2004). Recent advances in submarine slope surveys (e.g. Kelner et al., 2016; Clarke, 2018), sub-surface investigation (e.g. Brunet et al., 2016; Kuhlman et al., 2018), and modelling (e.g. Urlaub et al., 2015; Bellwald et al., 2019) have allowed submarine mass movement processes to be studied in unprecedented detail. Many of these recent studies have largely focused on determining why subaqueous mass movements initiate on low angled slopes (<2°) with gradients significantly less than the static angle of internal friction of their constituent materials (e.g. Urlaub et al., 2015), evacuating almost all the material from their source regions (Krastel et al., 2018; Mountjoy and Micallef, 2018), and often running out over long distances (c.10^1 to 10^2 km) (Talling et al., 2007). To explain their initiation and long runout, the presence of high pore fluid pressures that greatly exceed hydrostatic pressure is often postulated. Laboratory experiments and modelling indicate that these high pore fluid pressures could be generated through undrained cyclic loading during earthquakes (e.g. Sassa et al., 2012), the generation and retention of excess pore water pressures during sediment burial (e.g. Stigall and Dugan, 2010), focused fluid flow (e.g. Dugan and Flemings, 2000; Sassa et al., 2012) and/or gas liberation from hydrate dissociation (e.g. Riboulot et al., 2013).

The morphology of some subaqueous mass movements indicate they have displaced over much shorter distances before arresting, even when they are unconstrained downslope (Locat and Lee, 2002; Micallef et al.,

* Corresponding author.
E-mail address: j.carey@gns.cri.nz (J.M. Carey).

https://doi.org/10.1016/j.geomorph.2022.108247
Received 21 May 2021; Received in revised form 1 April 2022; Accepted 4 April 2022
Available online 9 April 2022

2013). In this case, landslide debris will be preserved on the slope within the landslide scar area and can potentially reactivate if stability conditions change (Fig. 1). These arrested landslides (defined as those that have moved a short distance relative to the landslide length) can often be observed close to sites where long run-out landslides have been initiated in a range of seafloor environments, including both passive margins and active margins that regularly experience seismic activity (Lee, 2009; Katz et al., 2015; Micallef et al., 2016).

Pre-conditioning (e.g. erosional undercutting, sediment loading, gas/fluid accumulation), triggering mechanisms (e.g. earthquakes, storms, fluid expulsion) and lithological controls (e.g. weak layers, vertical permeability variation) of submarine landslides are varied, complex and less well understood than terrestrial landslides. This is primarily due to the difficulties of accessing the seafloor and subseafloor, and that opportunities to link these preconditioning and triggering factors to submarine landslides at the time of slope failure events are rare (Hampton et al., 1996; Locat and Lee, 2002; Masson et al., 2006; Urlaub et al., 2015; Watson et al., 2020).

A significant knowledge gap lies in the potential for reactivation of arrested landslides, the quantification of reactivation mechanisms, and the mechanisms of resultant deformation. The likelihood of arrested landslides occurring in different environments (e.g., active vs passive margins, volcanic flanks) has received little attention. These gaps in knowledge constrain our ability to undertake reliable marine geohazard assessments (Nadim, 2006).

Many recent terrestrial landslide inventories (e.g. Li et al., 2014; Valagussa et al., 2016; Massey et al., 2018) also demonstrate that catastrophic landslides can occur close to landslides that show limited downslope movement, despite being subject to similar ground shaking intensities (Petley et al., 2006; Collins and Jibson, 2015). Given the failure characteristics of submarine slopes broadly match those found in terrestrial environments, it is anticipated that their potential movement mechanisms can be explored using similar techniques.

The mechanisms that control the rate and amount of movement of a low angled submarine landslide during dynamic loading can be explored through experiments using, for example, the dynamic back-pressured shearbox apparatus. Similar approaches have been adopted to accurately replicate dynamic loading scenarios in terrestrial landslide complexes during earthquakes and have shown how the shear surface deformation mechanisms can control movement patterns (e.g. Carey

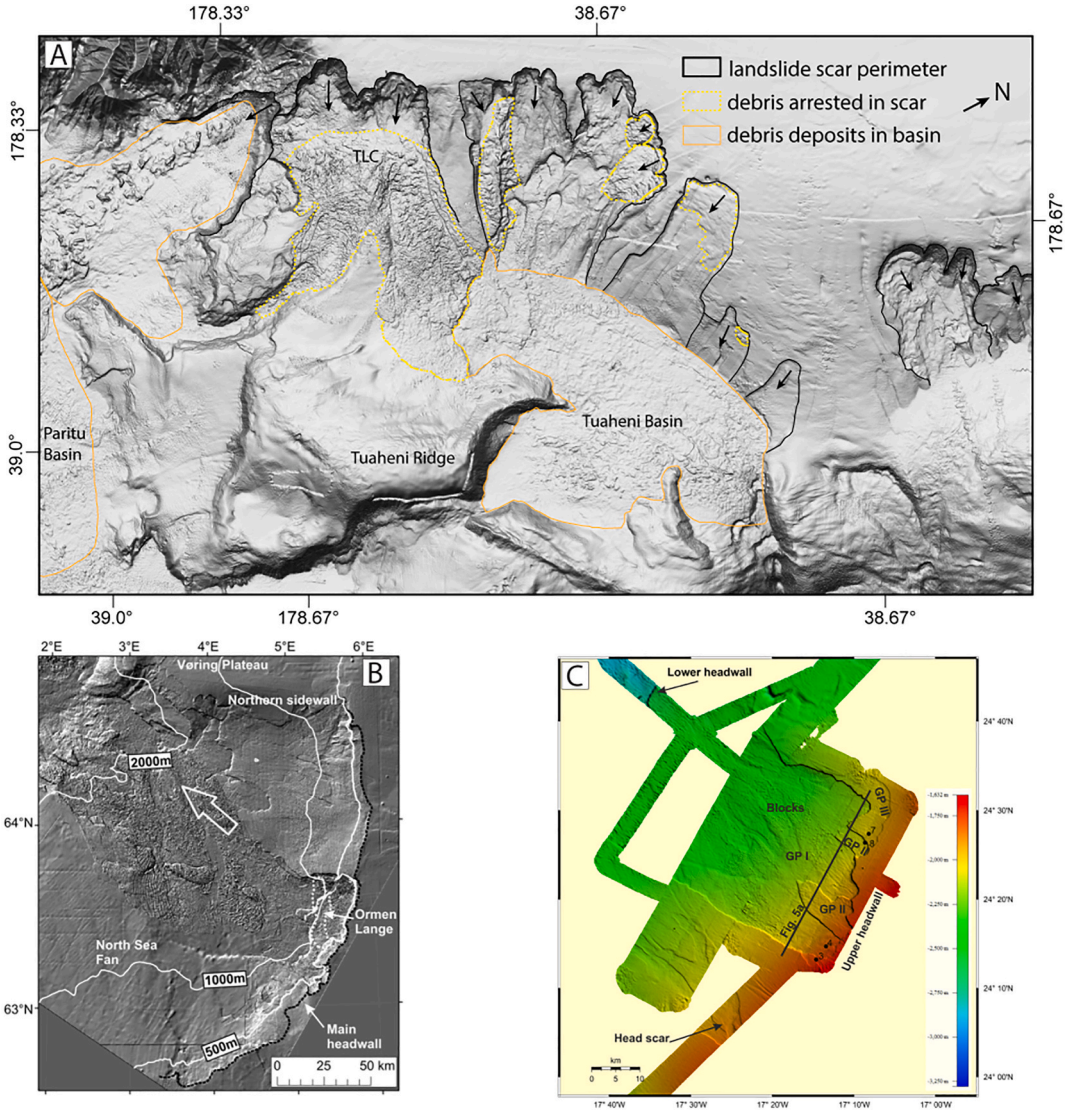

Fig. 1. Contrasting landslides that have debris arrested in the scar with those that do not. (A) Seafloor geomorphology of the wider TLC region showing numerous scars with little or no landslide debris (after Mountjoy et al., 2014). The TLC is unique here as almost the entire scar area contains landslide debris. (B) Additional example of a landslide with a significant volume of the debris remaining within the scar, the Storegga Slide (reproduced from Micallef et al., 2007). (C) Example of a landslide with very little debris remaining within the scar, the Sahara Slide (reproduced from Krastel et al., 2018).

et al., 2019a).

The Tuaheni Landslide Complex (TLC) is located in an active subduction zone that experiences regular seismic activity, on the Hikurangi Subduction Margin, off the coast of Gisborne, New Zealand (Fig. 2). Previous studies have confirmed that the TLC has a similar morphology to slow-moving terrestrial landslides (Mountjoy et al., 2009). Given that many terrestrial landslides moving on low-angled basal shear zones can remobilise episodically without catastrophic failure (e.g. Massey et al., 2013: Carey et al., 2019a) it has been postulated that the TLC may display a similar behaviour (Gross et al., 2018). The TLC, which has been investigated by both shallow coring and seafloor drilling (Kuhlman et al., 2018; Carey et al., 2019b; Pecher et al., 2019), is composed of subaqueous sediments common across the continental slope (Pecher et al., 2019). Although the TLC is known to experience regular seismic activity (Wallace and Beavan, 2010; Wallace et al., 2012), its potential movement response to earthquakes has received limited attention to date as alternative drivers for slope destabilization, in particular overpressure from free gas, have been the focus of investigations (e.g. Mountjoy et al., 2014; Micallef et al., 2016; Carey et al., 2019b).

Since we know that the Hikurangi margin experiences regular seismic activity, the aim of this study has been to investigate how low angled submarine landslides such as the TLC, might move when subjected to earthquake shaking. We have conducted laboratory experiments in a dynamic back-pressured shearbox on sediments recovered from the base of TLC to explore styles of movement under conditions that replicate seismic loading from recent local earthquakes, and from a potential future large subduction zone earthquake. We consider that a better understanding of the behaviour of the TLC provides insights into the movement mechanisms of other large low angled submarine landslides on both active and passive margins.

2. Study area

The Tuaheni Basin, located on upper continental slope on the Hikurangi Subduction Margin, hosts a number of submarine landslides (Mountjoy et al., 2009; Micallef et al., 2016; Watson et al., 2020) The TLC (Fig. 2), which covers a surface area of approximately 145 km^2, can be sub-divided into two distinct geomorphological units (termed Tuaheni North and Tuaheni South), which are separated by a 2 km wide unfailed spur (Fig. 3 A). Whilst Tuaheni North is characterized by multiple evacuated landslide scarps, Tuaheni South is comprised of a large debris apron that has a distinct scarp and bench topography, and features indicative of lateral shear, extensional and compressional deformation (Mountjoy et al., 2009, 2014; Couvin et al., 2020). The morphology of Tuaheni South is broadly similar to that of slow-moving landslide complexes observed in terrestrial environments, such as earthflows and mudslides (e.g. Hungr et al., 2014), which occur in similar fine-grained sediments and are often subject to episodic

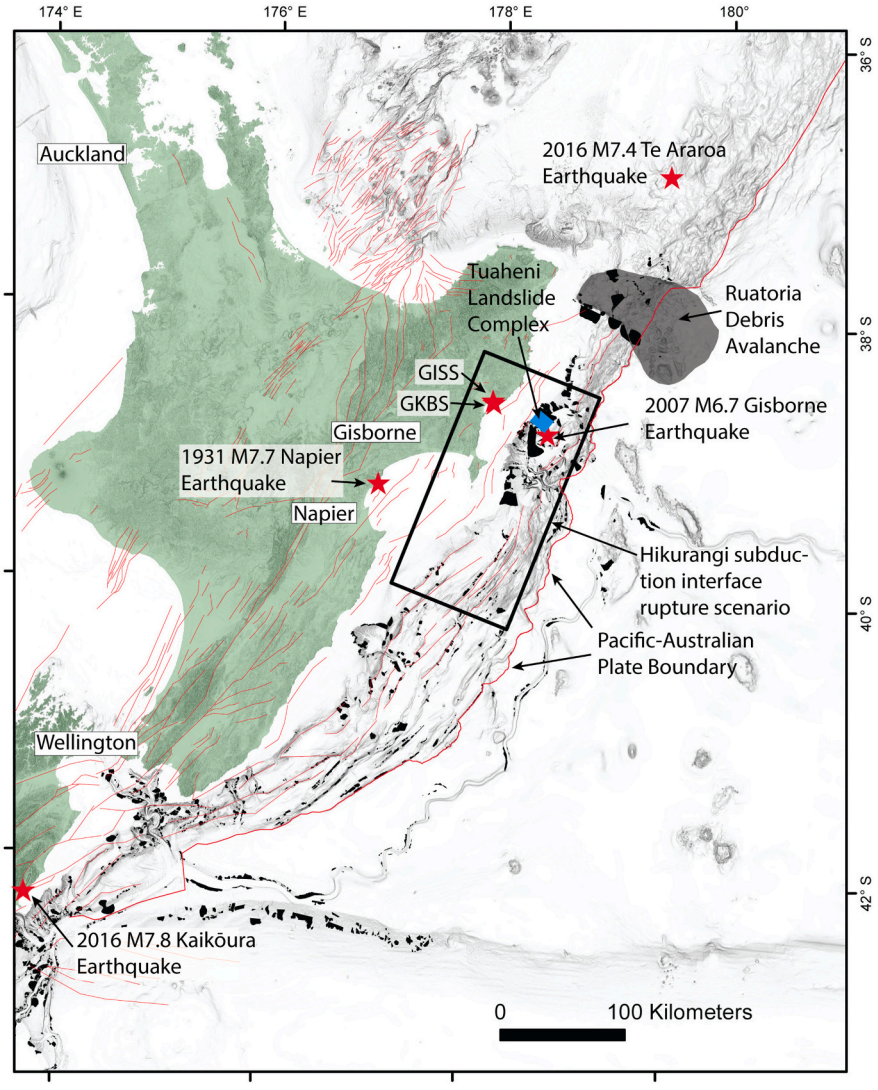

Fig. 2. The location of The Tuaheni Landslide Complex (blue box) on the Hikurangi Margin off the east coast of the North Island of New Zealand in relation to other mapped submarine landslides (black polygons) (Watson et al., 2020) and onshore and offshore faults (red lines) (Litchfield et al., 2014). Recent onshore and offshore earthquakes epicenters (red dots) have been recorded at nearby stations (GISS and GKBS) on the GeoNet network. (For interpretation of the references to colour in this figure legend, the reader is referred to the web version of this article.)

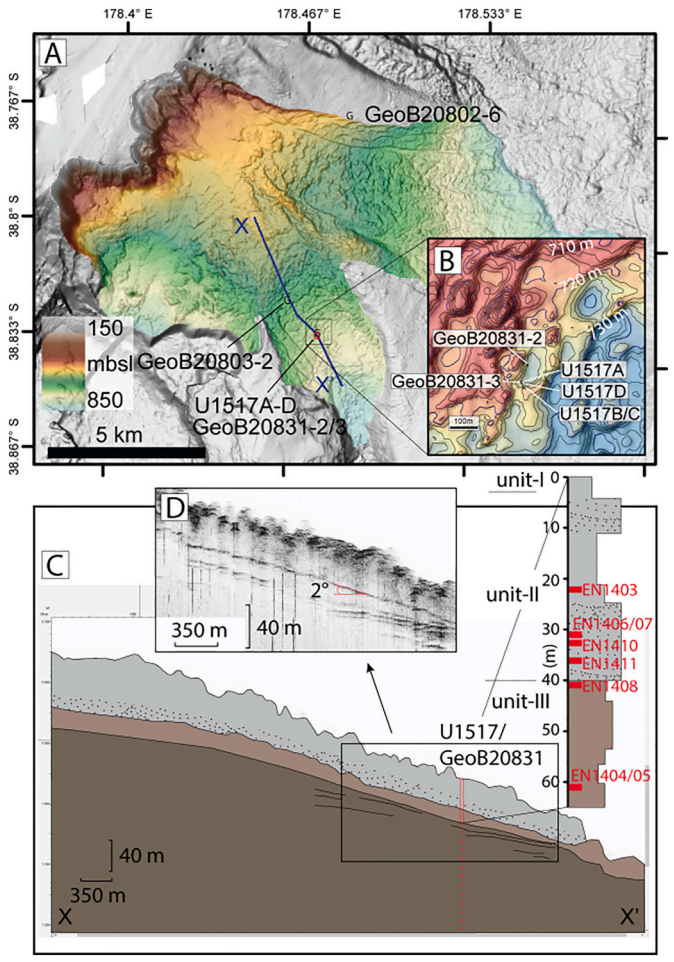

Fig. 3. (A) The morphology of the TLC determined from 20 m resolution bathymetry (coloured part of the seafloor). Also shown are borehole locations drilled during RV Sonne Mebo expedition SO247 (Sites GeoB20802 and GeoB20831) and IODP Expedition 372 (Site U1517). (B) Detailed bathymetry and bore hole locations within the landslide. (C) Two-dimensional landslide cross section interpreted from seismic data (Barnes et al., 2019a, 2019b; Couvin et al., 2020) illustrating the three major sedimentary units (grey = Units I and II, light brown = Unit III, dark brown = Unit IV). Red lines in the inset stratigraphic column represent the locations of samples used in this study. (D) Sub-bottom profiler data showing the low-angled (approximately 2°) basal shear zone. (For interpretation of the references to colour in this figure legend, the reader is referred to the web version of this article.)

remobilisation (e.g. Allison and Brunsden, 1990).

The upper continental slope is composed of Miocene to Recent slope basin sequences (Mountjoy et al., 2009). Gravity cores collected across the TLC have indicated that the upper few meters of sediment are dominated by mud to sand sized particles from hemipelagic drape, reworked landslide debris and airfall tephra (Kuhlman et al., 2018). Sediments from the base of the TLC have been recovered from boreholes drilled during the RV Sonne Mebo expedition SO247 (Fig. 3 A and B, Holes Geo20802 and Geo20831) in 2016 and during IODP Expedition 372 in 2017/2018 (Fig. 3 A, Hole U1517C). Whilst seismic interpretation suggests that the base of the landslide at Site U1517 is approximately 40 m below seafloor (bsf) (Couvin et al., 2020), the undrained shear strength data at Hole U1517C indicate a drop in shear strength around 25 m bsf, which may point to a shallower shear zone (Barnes et al., 2019a) A recent core log seismic integration study further highlighted the difficulty in identifying the basal shear throughout the landslide complex (Crutchley et al., 2022). These boreholes demonstrate that the base of the landslide is dominated by fine grained sandy sediments. The base of the landslide was found to be at least 70 m above the base of gas hydrate stability at Hole U1517C (Fig. 3 C and D), indicating that the development of overpressure from free gas in this region is unlikely (Pecher et al., 2019; Screaton et al., 2019). Furthermore, initial analysis of in-situ pore pressure measurements below the landslide indicated hydrostatic conditions (Barnes et al., 2019b). With no evidence for formation overpressure as a driving mechanism, the development of transient overpressure during seismic loading from earthquakes is a credible mechanism that could drive landslide movement.

Regional seismic hazard is characterized by earthquakes on shallow crustal faults (such as the 1931 Napier earthquake), on the Hikurangi subduction zone interface (up to ten large earthquakes in the last 7000 years, Clark et al., 2019), and on intraslab faults (such as the 2007 M6.7 Gisborne event (GEq)). In addition, the Tuaheni Basin is prone to moderate intensity but long duration shaking from large distant events (such as the 2016 M7.8 Kaikōura (KEq) and 2016 M7.4 Te Araroa (TAEq) earthquakes) (Kaneko et al., 2019). Ground shaking in the Tuaheni Basin can be subjected to strong amplification at periods of about 20 s from the deep offshore sediment basin (Kaneko et al., 2019) and result in the triggering of submarine landslides (Howarth et al., 2021). However, these are unlikely to influence dynamic triggering of the TLC, which has a natural frequency estimated between 0.5 and 5 Hz considering the varying material properties and landslide thickness (25–50 mbsf) (Singh et al., 1988).

3. Methods

3.1. Simulating ground shaking scenarios

To determine a range of representative ground shaking scenarios at the TLC we derived "stressgrams" (described later) from seismograph data for three recently recorded earthquakes and calculated synthetic ground motions for a plausible future magnitude 8.2 subduction zone earthquake (Fig. 4). Whilst shallow earthquakes can trigger large surface waves which are typically long period (<0.2 Hz), this study focused on movement triggered by body waves that have similar frequencies to the natural period of the landslide (+0.5 Hz).

Given no seismometers have been installed offshore near the TLC, we employed two approaches to obtain indicative peak shaking values for the recent earthquakes. First, for the distant earthquakes TAEq and KEq with epicentral distances of ~230 and ~450 km respectively, we assume that peak shaking at the landslide site will be similar to peak shaking at an onshore station 30 km away (GKBS - GeoNet network, Fig. 2). Ground shaking at a site is affected by local source effects, regional geology (attenuation) and local site effects (shallow soil) (Lay and Wallace, 1995). Given the TLC is far from earthquake source for TAEq and KEq, seismic recordings on nearby rock sites provide an appropriate analogue of the shaking input at Tuaheni. GKBS is a rock site located with a site-class B type soil condition, equivalent to a strong rock with little site amplification. Three-component velocity seismograms obtained for both TAEq and KEq were integrated from recorded accelerograms at station GKBS. The velocity seismograms have been bandpass filtered between 0.5 and 5 Hz. In this study we convert seismograms into stressgrams using the relationships described by Cox et al., 2015, to estimate dynamic stress conditions (σ) at the base of the landslide. Stressgrams are better input parameters to model the various landslide responses and were derived using the following equation:

$$\sigma = (\mu s \cdot V/Vs) \quad (1)$$

where V is velocity seismogram, μs is the material shear modulus (estimated from published data on similar marine sediments with comparable density characteristics in Schumann et al., 2014 as 0.65 GPa) and Vs is the material shear wave velocity (calculated from the estimated shear modulus and material bulk density (1.9 g cm^{-3}) as

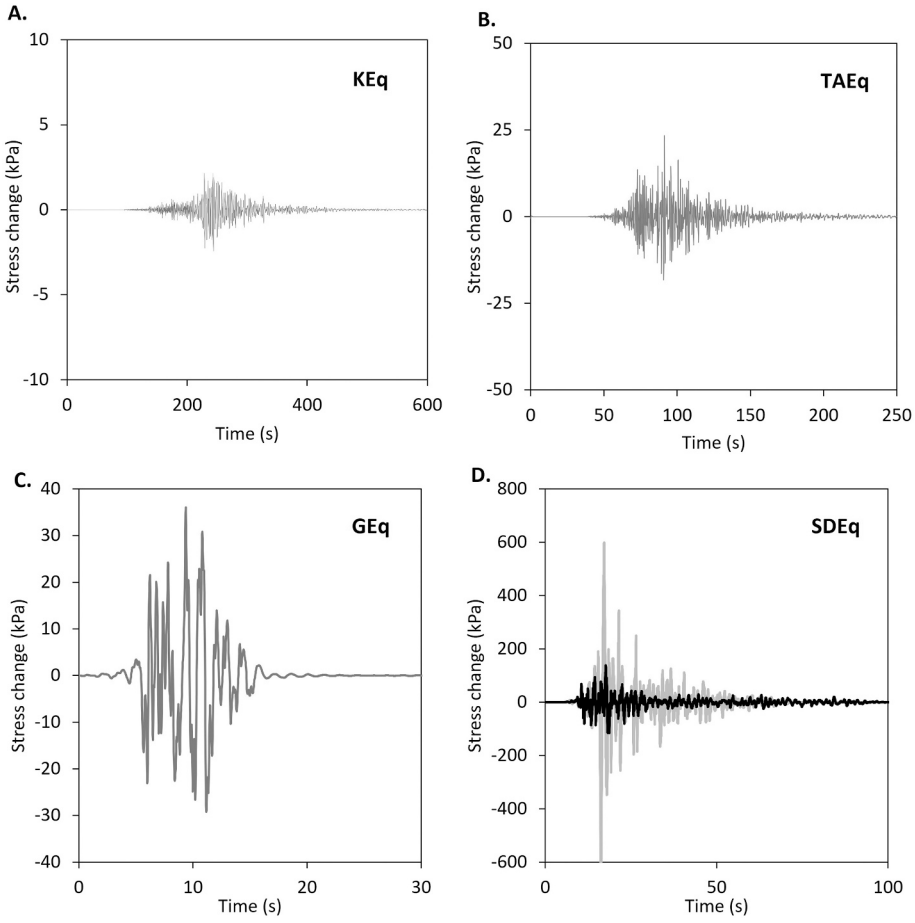

Fig. 4. Earthquake induced dynamic stress changes (East-west component) derived from recorded or simulated data at the TLC (filtered between 0.5 and 5 Hz) for: (A) M7.8 Kaikoura Earthquake (KEq), recorded at the GeoNet Gisborne station (GKBS, Fig. 1), 2016; (B) M7.1. Te Araroa earthquake (TAEq), recorded a the GeoNet Gisborne station (GISS, Fig. 1), 2016; (C) M6.7 Gisborne earthquake (GEq), 2007, modelled at the TLC, and (D) Magnitude 8.3 subduction earthquake (SEq) modelled at the TLC for selected seismograms representing lower bound (NW 3 MPa stress drop 0 – dark grey) and upper bound (SE 9 MPa stress drop – light grey) amplitudes.

584.9 m s^{-1}). The final stressgrams have been halved to remove the free surface effect from the original velocity seismogram (Fig. 4 A and B) to allow for comparison with the dynamic shear experiments.

For the local earthquake GEq we considered it to be more appropriate to calculate synthetic ground shaking as the ground shaking at nearby sites can differ due to local source and wave propagation patterns. We computed ground motion simulations to model GEq stressgrams at TLC using EXSIM, a finite fault stochastic modelling code that considers finite fault parameters as well as regional parameters (Motazedian and Atkinson, 2005). The stochastic approach requires a well-defined source model, attenuation model, and quantification of site effects. These parameters, as well as the validation method, are provided in the supporting information (S1). This method provides realistic waveform duration, amplitude and frequency content. Synthetic horizontal accelerations were integrated into velocity, which was bandpass filtered between 0.5 and 5 Hz and converted into stressgrams (Fig. 4 C).

To evaluate the ground shaking potential at the site during a future large Hikurangi subduction zone earthquake we computed synthetic ground motions at TLC. Following Holden et al. (2017) we have developed plausible rupture scenarios of large magnitude 8.3 subduction earthquakes in the area of interest, constrained onto a 200 × 100 km^2 interface area offshore Hawkes Bay following a central Hikurangi margin segment model from Stirling (2012) (estimated 1400 yr recurrence interval) and a recent study by Clark et al. (2019) characterized by:

(i) heterogeneous slip distributions;
(ii) 4 hypocentral locations; and
(iii) the level of stress drop appropriate for large subduction earthquakes.

We generated twelve source scenarios with magnitude Mw8.3 and employed EXSIM, taking into account finite fault parameters of the segment of interest as well as regional parameters validated above (See Supporting information, S1). We varied hypocenter locations on the rupture plane (SE, SW, NE and NW) and stress drops (3, 6 and 9 MPa) for random slip distributions. Horizontal accelerations were then calculated at TLC, filtered, integrated into velocities, and then converted into stressgrams (Fig. 4 D).

3.2. Laboratory testing

We conducted a suite of conventional laboratory experiments on TLC sediment samples collected from boreholes GeoB20831 (from Sonne Expedition SO247 in 2016 – Huhn, 2016) and U1517 (from IODP Expedition 372 in 2017 – Barnes et al., 2019a) (Fig. 3 A) to determine their physical and geomechanical characteristics (Table 1).

Index testing demonstrated that whilst natural moisture contents were broadly consistent (23% to 27%) across all samples, the landslide is composed of two distinct sediment types (Table 1). Samples EN1403, EN1404, and EN1408 can be classified at the boundary of low plasticity silts and clays, characterized by lower bulk and dry densities, higher liquid limits and plasticity indexes (Table 1). In contrast, samples EN1407, EN1409, EN1410 and EN1410 can be classified as fine sands, characterized by high bulk and dry densities, lower liquid limits and plasticity indexes (Table 1). The bulk density, dry density and moisture contents measured on the laboratory samples (Table 1) were found to be consistent with the measurements made at Sites U1517C and Geo20832 (Fig. 5). Particle-size analyses was undertaken using a Beckman Coulter LS13320 laser mastersizer with 92 size bins from 2 mm to 0.375 μm. This confirmed two distinct grain size distributions with coarse silt and

Table 1
Physical properties of TLC sediments recovered from boreholes GEOBORE 20831-3 and IODP U1517.

Sample reference	EN1403	EN1404	EN1405[b]	EN1406[b]	EN1407	EN1408	EN1409	EN1410	EN1411
Borehole	U1517	U1517	U1517	U1517	U1517	U1517	20831-3	20831-3	20831-3
Sample depth ([a]mbsf)	21.44–21.53	61.26–61.38	59.20–59.30	30.06–30.22	31.61–31.77	40.69–40.80	28.40–29.60	31.90–33.27	35.40–36.92
Moisture content (%)	27.2	23.0	–	–	24.6	26.9	23.3	23.3	24.3
Bulk density (g/cm^3)	1.82	1.83	–	–	1.89	1.89	1.99	2.03	1.85
Dry density (g/cm^3)	1.43	1.49	–	–	1.54	1.49	–	–	1.48
Atterberg limits									
Plastic limit (%)	28.0	20.0	–	–	25.2	22.1	23.1	26.4	23.1
Liquid limit (%)	48.1	38.5	–	–	33.2	43.4	34.2	31.8	34.3
Plasticity index (%)	20.1	18.5	–	–	8.0	21.3	11.2	5.4	11.2

[a] mbsf = meters below seafloor.
[b] Samples not used for index testing.

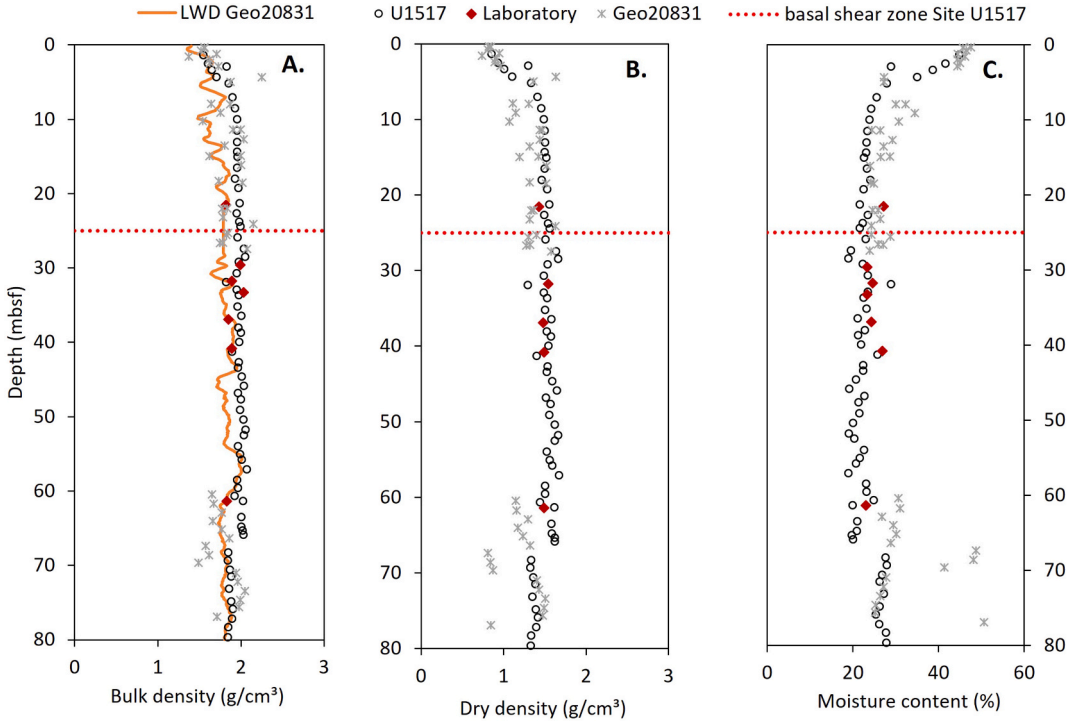

Fig. 5. Comparison of physical properties measured at various depths up to 80 m during the RV Sonne Mebo expedition SO247 at Site Geo20831 in 2016, the IODP Expedition 372 at Site U1517 in 2017/2018 and in laboratory during this investigation (A) Bulk density (B) Dry density (C) Moisture content.

fine sands accounting for over 80% of the material in the coarse-grained sediments, and silts and clays accounting for over 80% of the material in the fine-grained sediments (Fig. 6).

Conventional monotonic drained direct shear tests were undertaken on 60 × 60 × 20 mm intact fine sands sediment samples using a Wykeham Farrance WF2500 direct shearbox following standard procedures (BSI, 1990). The samples were consolidated at three different normal stresses (32 kPa, 153 kPa and327 kPa) selected to span a range of potential shear surface depths up to 40 m bsf (Barnes et al., 2019a; Couvin et al., 2020; Crutchley et al., 2022). On completion of each consolidation phase shearing was initiated at a low shear rate (0.024 mm min^{-1}) to avoid the development excess pore fluid pressures within the specimens.

The drained shear test results were used to design a suite of dynamic direct shear experiments to explore the behaviour of the fine sand sediments within the TLC during seismic loading. These experiments were undertaken in a Dynamic Back Pressured Shear Box (DBPSB), an advanced direct shear device that allows the measurement and control of pore pressures and dynamic application of normal stress and shear stress, which has been successfully used to explore a range of styles of deformation in landslide materials (e.g. Brain et al., 2015; Carey et al., 2016, 2019a). These experiments were conducted on intact and reconstituted fine-grained sediments from samples EN1409 and EN1410 (Table 2). Reconstituted samples were initially oven dried and then sieved to remove any over-sized particles before being mixed with de-aired water to a representative intact water content (approx.. 25.5%). To ensure each experiment had a uniform initial bulk density within the range measured in the intact fine-grained sand samples (Table 1), the samples were lightly compacted in layers within a compaction mould.

To evaluate the most appropriate testing methodology to simulate undrained cyclic loading in the coarse silt and fine sand sediments at the base of the TLC during earthquakes we conducted two strain controlled dynamic shear experiments on samples EN1409A and EN1410B (Table 2). Each sample was consolidated at a normal effective stress of 150 kPa, to represent an approximate 25 m bsf calculated from logging whilst drilling (LWD) density data at Site U1517 (Barnes et al., 2019a, 2019b) using the following equation.

$$\sigma_n' = \gamma' H \quad (2)$$

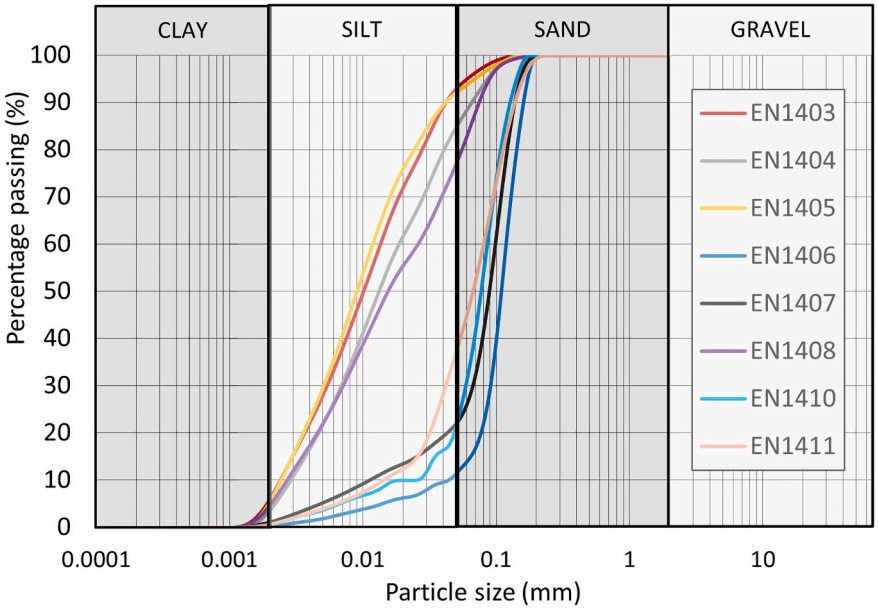

Fig. 6. Particle size analysis of samples recovered from within the Tuaheni Landslide Complex.

Table 2
Summary of the dynamic direct shear experiments.

Sample number	Intact/ reconstituted	Initial normal effective stress (kPa)	Initial bulk density (g/cm^3)	Initial shear stress (kPa)	Applied dynamic shear amplitude (±)	Applied normal stress	Dynamic frequency (Hz)	Number of cycles
EN1409A	Intact	150	1.85	64	0.5 mm	150 kPa	0.5	30
EN1410B	Reconstituted	150	1.90	64	0.5 mm	Volume controlled	0.5	30
EN1410C	Reconstituted	150	1.93	10	25 kPa	Volume controlled	0.5, 2, 5	10
EN1410D	Reconstituted	150	1.93	10	10,25,50 60 kPa	Volume controlled	0.5	30

where σ_n' is the normal effective stress; γ' is the effective unit weight calculated from LWD density data and assuming a sea water density of 1030 kg m^{-3} and H is the sub-sea-floor depth. The 25 m sub-seafloor depth coincides with a significant reduction in shear strength that may represent the basal shear zone of the landslide at Site U1517 (Crutchley et al., 2022). After consolidation, an initial static shear stress of 65 kPa (approximately 70% of the conventional drained failure envelope) was applied to each sample to ensure the shear zone was in a stress state close to (but not at) failure prior to dynamic shearing. Two different methodologies were used to determine how best to simulate the undrained failure behaviour anticipated during seismic loading. Sample EN1410A was subjected to the testing approach successfully used by Carey et al. (2016) to induce liquefaction in loess sediments. In this experiment the normal stress and back pressure were held constant as a strain controlled dynamic shear was applied to the sample whilst the development of excess pore water pressure and shear stress were measured (Fig. 7 A and B). Conversely, Sample EN1410B was subjected to an experimental procedure adapted from a well-established sample volume-controlled dynamic simple shear experiment (Dyvik et al., 1987). In this experiment, a constant sample volume was applied during dynamic shear by maintaining a constant sample height (axial displacement) and pore fluid volume (back volume) such that the reduction in mean effective stress resulting from the reduction in applied normal stress was equal to the excess porewater pressure that would have been generated in a purely undrained experiment (Fig. 7 C and D).

Once the preferred experimental approach had been determined (see below) two further experiments were undertaken on reconstituted samples EN1410C and EN1410D to simulate dynamic loading at shear stress representative within the low-angled basal shear zone of the TLC. In these experiments the same initial normal effective stress was applied to each sample during consolidation (150 kPa) whilst a lower initial shear stress of 10 kPa was applied to each sample (Table 2) to represent the stress state extant in the TLC. This initial shear stress was estimated using the following equation:

$$\tau = \gamma' H sin\alpha cos\alpha \quad (3)$$

where τ is the shear stress; γ' is the effective unit weight; H is the shear surface depth from the sea floor, and α is shear surface angle (c. 2–4°) identified in geophysical interpretations of the landslide geometry (Gross et al., 2018). The initial pore water pressure was set to simulate hydrostatic conditions.

To explore the deformation behaviour of the TLC when subject to different frequencies of short duration, dynamic loading, sample EN1410C was subject to three separate dynamic stress-controlled shear stages (Table 2). In each case dynamic shear stress was applied over 10 cycles at progressively higher frequencies (Table 2). The initial normal effective stress and shear stress was reapplied to the sample between each dynamic shear stage (Fig. 9 A, Table 2). To evaluate the displacement behaviour of the TLC during periods of longer duration dynamic loading, sample EN1410D was subjected to four dynamic shear stages at a frequency of 0.5 Hz for a duration of 60 s (30 cycles). As in experiment EN1410C, the initial normal effective stress and shear stress were applied to the sample between each dynamic shear stage whilst the amplitude of applied shear stress was increased at each stage (Table 2, Fig. 10 A).

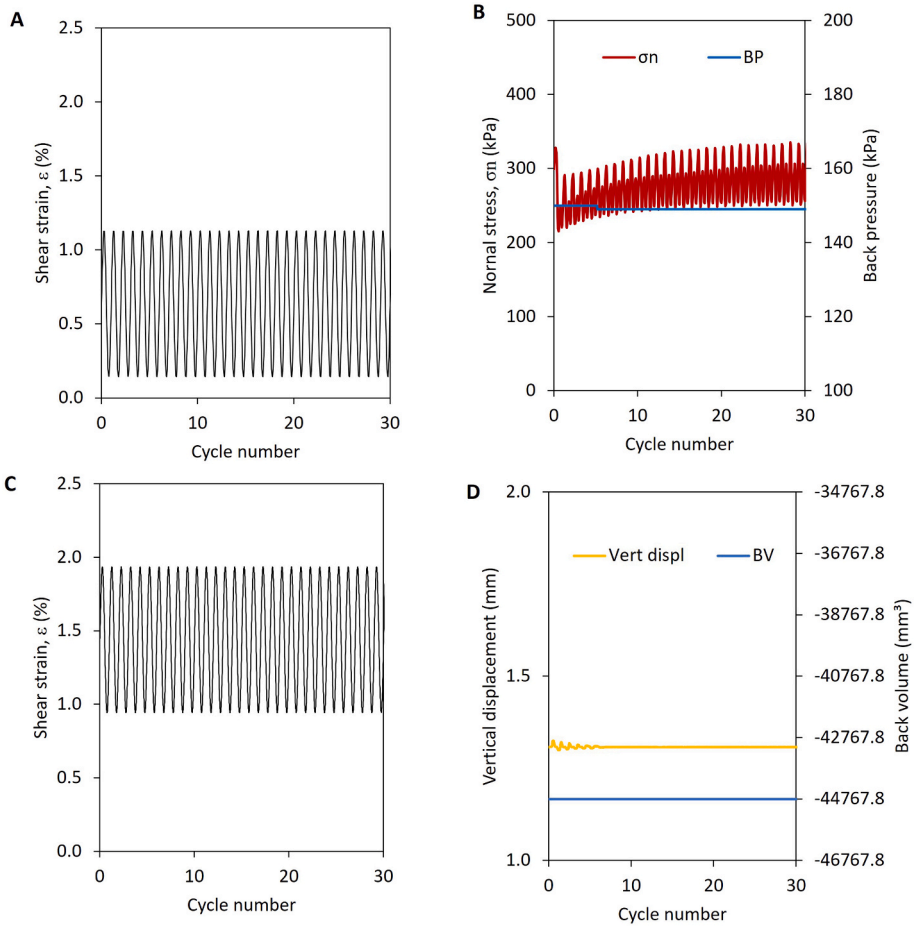

Fig. 7. Dynamic strain controlled shear experimental approaches adopted to generated undrained behaviour in response to dynamic loading. On samples EN1409A and EN1410B (A) Applied dynamic shear strain during the normal stress controlled experiment conducted on sample EN1409A (B) Applied Back pressure (BP) and normal stress (σn) during normal stress controlled experiment conducted on sample EN1409A (C) Applied dynamic shear strain during the volume controlled experiment conducted on sample EN1410B (D) Constant normal displacement a back volume (BV) applied to during the volume controlled experiment conducted on sampleEN1410B.

4. Results

The conventional drained shear tests produced a linear monotonic strength envelope (Fig. 8 A and B) with $\phi' = 32.5°$ and $c' = 15$ kPa for peak strength, and $\phi' = 29.2°$ and $c' = 0$ for residual strength. Undrained shear strengths calculated from onboard shear vane tests at Site U1517 are broadly consistent with the monotonic strength envelope (Fig. 8 B). The strength characteristics were lower than those measured for fine-

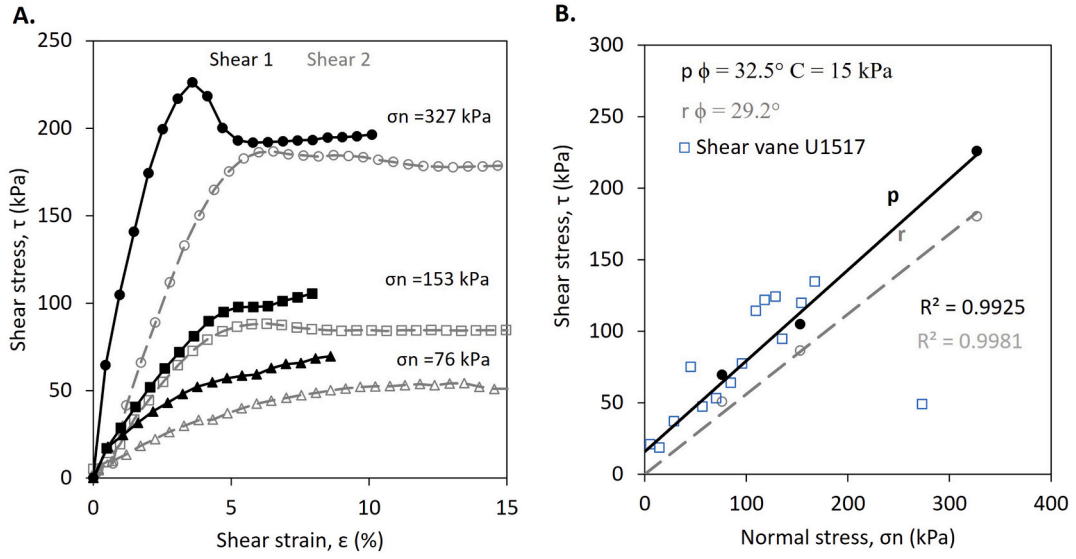

Fig. 8. Conventional monotonic drained shear experiment results. (A) Stress-strain behaviour. (B) Monotonic drained peak and residual strength envelopes plotted with the undrained shear strength measured using a shear vane apparatus at Site U1517. Note: normal stresses for undrained shear strength data are estimated from borehole depths and an average bulk density of 1.9 g/cm^3. Peak strength envelope (p) calculated as linear best fit and residual strength envelope (r) calculated as linear best fit assuming 0 kPa cohesion.

grained pelagic silts and clays tested during previous studies of the TLC, which were sampled in shallow seafloor cores (Carey et al., 2019b).

During the normal stress-controlled experiment (EN1409A) dynamic strain-controlled shear resulted in a decrease in sample pore water pressures and an increase in normal effective stress (Fig. 9 A). Consequently, continued sample strain required a progressive increase in shear stress throughout the experiment (Fig. 9 A). The experiment did not generate undrained conditions in the sample, which instead followed a drained stress path and resulted in sample densification and subsequent strain hardening (Fig. 9 B).

During the volume-controlled experiment (EN1410B), dynamic shear resulted in a rapid reduction in mean effective stress over the first 10 cycles of loading, indicating the development of significant excess pore water pressures (Fig. 9 C). This reduction in normal effective stress corresponded with a rapid loss in shear strength until no significant frictional strength could be measured (Fig. 9 C). The stress path indicates that the failure envelope was reached during the first dynamic cycle and during further cycles the stress path followed the residual failure envelope as the sample underwent liquefaction (Fig. 9 D).

This experiment demonstrates that the fine sand forming the basal material of the TLC is prone to liquefaction as a result of seismic loading when subject to the requisite strain conditions. The volume-controlled experiments were able to replicate the undrained behaviour expected in the landslide shear zone during seismic loading. Consequently, this testing approach was adopted to further explore the potential movement behaviour of the TLC during earthquakes of varying magnitude and duration.

During the first low frequency dynamic shear stage on sample EN1410C (0.5. Hz) dynamic loading resulted in progressively larger shear strains, although the total cumulative shear strain was comparatively small (c. 1.5%) (Fig. 10 A and B). These progressively increasing shear strain cycles developed as the normal effective stress reduced (Fig. 10 C), indicating that the sample was strain softening during dynamic loading prior to reaching the conventional monotonic failure envelope (Fig. 10 D). Lower shear strains were then measured during the second dynamic shear stage (<0.5%) (2 Hz) despite a similar reduction in normal effective stress during dynamic loading. Similar behaviour was also observed during the third dynamic shear stage (5 Hz), which was accompanied by a much lower reduction in mean effective stress during dynamic loading, suggesting that the sample progressively strengthened between each dynamic stage as the initial normal stress was reapplied and pore fluids.

The results indicate that whilst short duration dynamic shear stages could induce shear strain and excess pore water pressure development, the reduction in normal effective stress was not sufficient to reach the conventional failure envelope, preventing the generation of significant permanent displacement or liquefaction (Fig. 10 D).

The longer duration dynamic loading applied to sample EN1410D (Fig. 10 A) demonstrated that low amplitudes of dynamic shear stress (±10 kPa) resulted in no permanent displacement (Fig. 11 B) or measurable reduction in mean effective stress (Fig. 11 C). Only minor changes in the stress path were observed during this stage of dynamic loading as the sample remained in a stable state (Fig. 11 D). During the next dynamic shear stage (±25 kPa) (Fig. 11 A), significant permanent displacement was observed (Fig. 11 B). During this stage, dynamic loading resulted in a rapid reduction in mean effective stress (Fig. 11 C) until the failure envelope was reached ($\sigma n' = 0$ kPa $\tau = 25$ kPa) after approximately 20 cycles (Fig. 11 C). Once the failure envelope was

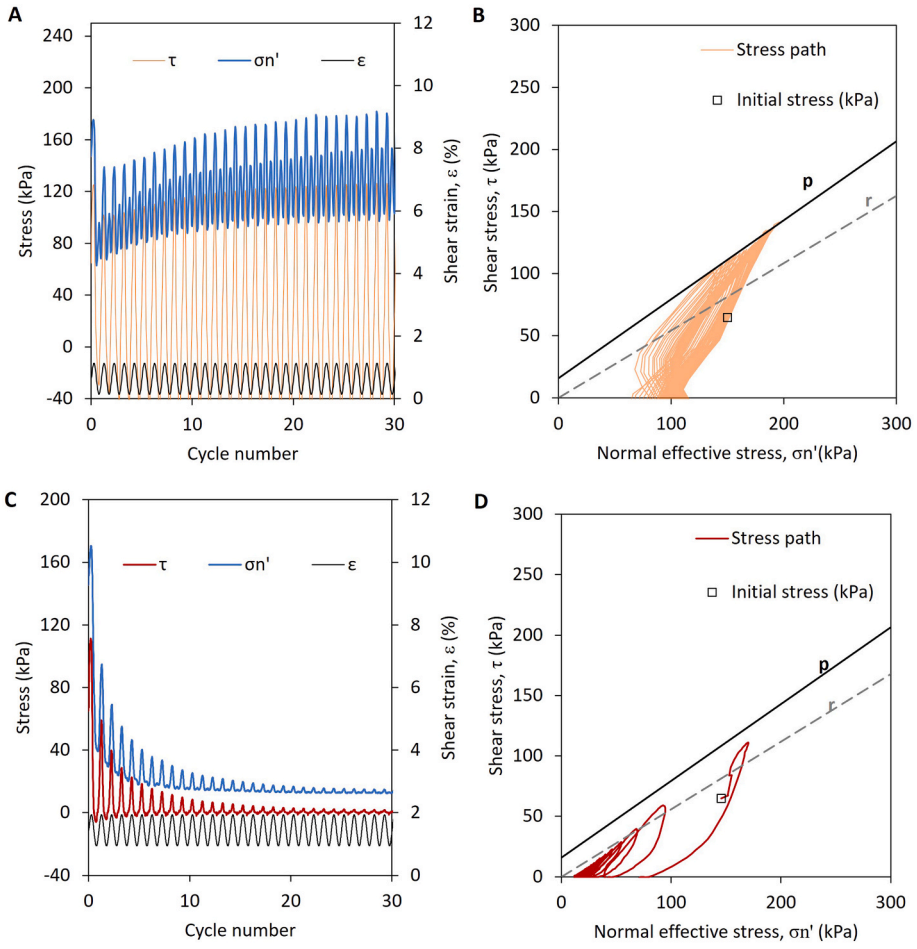

Fig. 9. Strain controlled dynamic shear experiments (±0.5%) conducted at a frequency of 2 Hz. (A) Shear stress (τ) Normal effective stress (σn′) and Shear strain (ε) against cycle number during normal stress controlled dynamic shear experiment, Sample EN1409A (B) Stress path in relation the peak (p) and residual (r) monotonic failure envelope, sample EN1409A. (C) Shear stress (τ) Normal effective stress (σn′) and shear strain (ε) plotted against cycle number during sample volume controlled dynamic shear experiment, Sample EN1410B. (D) Stress path in relation the peak (p) and residual (r) monotonic failure envelope, sample EN1410B.

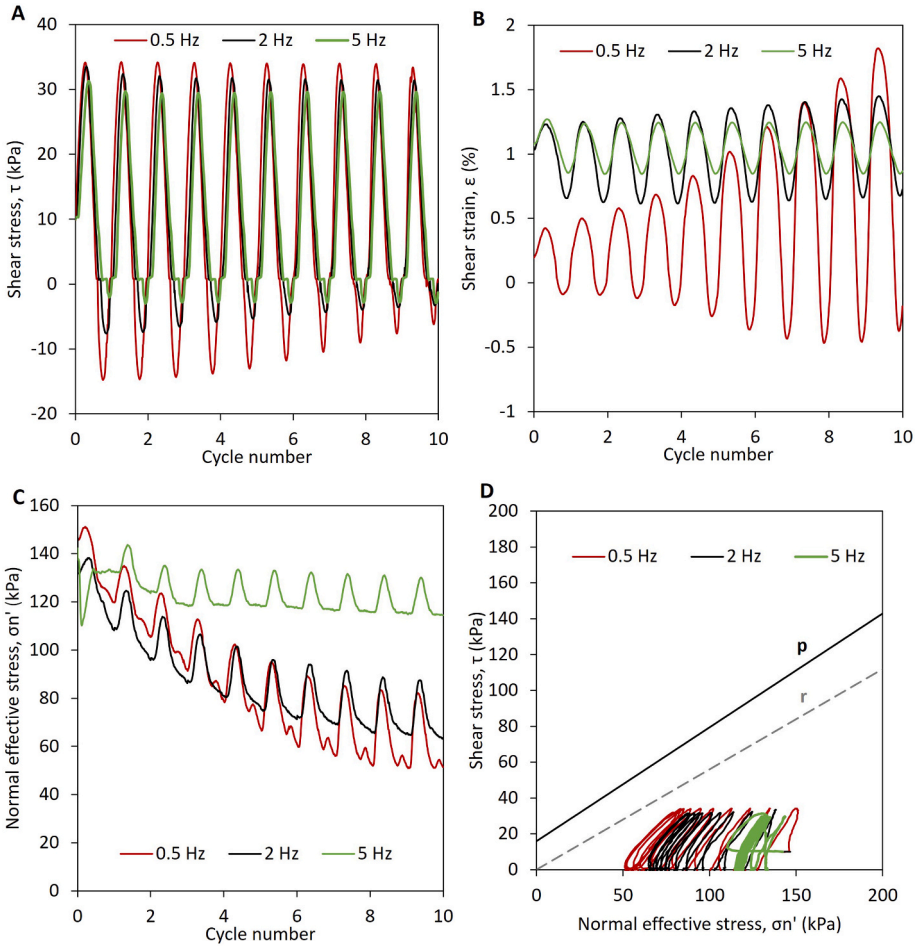

Fig. 10. Short duration dynamic shear experiments (10 cycles) conducted at a shear stress amplitude of 25 kPa and frequencies 0.5 Hz, 2 Hz and 5 Hz on sample EN1410C (A) Applied shear stress (τ) (B) Measured shear strain (ε) (C) Normal effective stress (σn′) (D) Stress path in relation to the peak (p) and residual (r) monotonic failure envelopes.

reached the shear displacement and a slight reduction in shear stress was observed as applied shear stress could no longer be sustained (Fig. 11 A). This reduction in shear stress, however, did not result in liquefaction as the shear stress remained at the failure envelope (approx. 20 kPa, Fig. 11 A, D). Further dynamic shear stages at higher amplitudes (±50 kPa and 60 kPa) produced the same undrained loading behaviour. In both stages, dynamic shear resulted in undrained loading, characterized by a rapid reduction in mean effective stress and shear displacement once the failure envelope was reached. Although the increase in dynamic shear stresses generated larger shear displacement as the failure envelope was reached, only a moderate reduction in shear stress was observed (Fig. 11 A, D), which indicated that the sample could maintain some shear strength rather than undergoing liquefaction (Fig. 11 D).

The results demonstrate that, whilst the excess pore water pressures generated during the longer duration dynamic shear experiment were sufficient to reach the failure envelope, they did not result in liquefaction or runaway failure in any of the loading scenarios tested. Instead, the experiments showed that the shear surface began to displace once the normal effective stress reduced to the conventional failure envelope. Shear displacement terminated at the end of dynamic shearing and remobilised by the same mechanism during subsequent dynamic shear stages once the failure envelope was reached. This behaviour is consistent with a conventional frictional sliding model (e.g. Helmsetter et al., 2003) with no evidence of rate dependency effects.

5. Discussion

A range of mechanisms have been proposed to explain subaqueous mass-movement, including shear surface nucleation (e.g. Viesca and Rice, 2012); shear zone liquefaction and ductile extrusion (e.g. Bull et al., 2009; Sassa et al., 2012); local lateral fluid flow (Dugan and Flemings, 2000; Flemings et al., 2002), and the development of high pore fluid pressures (and thus low effective stress states) by free gas (Carey et al., 2019b). Few mechanisms, however, have been proposed to explain the presence of arrested submarine landslide complexes subject to large earthquakes. In this study we have undertaken a suite of dynamic shear experiments to explore the potential movement mechanisms in large submarine landslide complexes that are subject to regular seismic loading events of varying magnitude and duration.

Initial experiments demonstrated that the fine-grained sandy sediments at the base of the TLC have the capacity to undergo liquefaction under appropriate stress states. However, at simulated stress states that represent the low angled (approx. 2°) basal shear zone in the landslide, liquefaction did not occur. Instead, permanent deformation occurs through displacement along the shear surface when the material's friction strength is exceeded. This occurs once the monotonic failure envelope is reached or exceeded by a decrease in mean effective stress associated with the development of excess pore water pressures (Fig. 12).

During both long and short duration dynamic experiments in which shear stresses remained low the sediments were unable to generate high excess pore water pressures (Fig. 12, stress path 1). As a consequence,

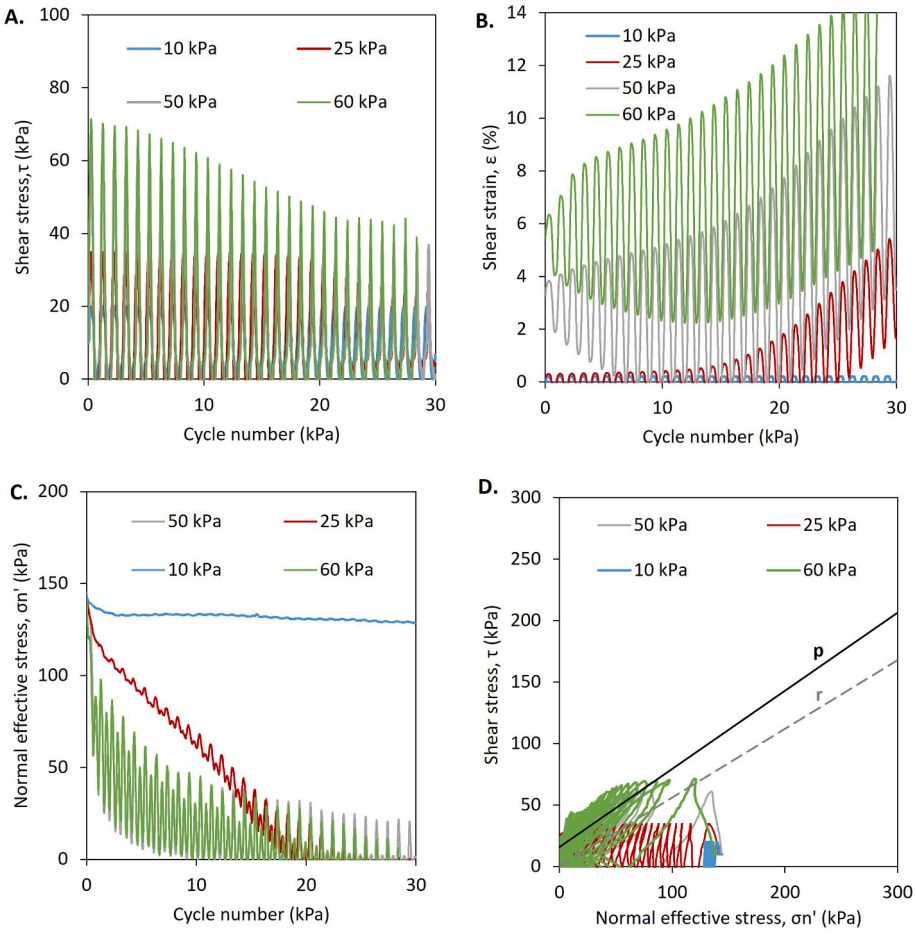

Fig. 11. Long duration dynamic shear experiments (30 cycles) conducted at a frequency of 0.5 Hz at different applied dynamic stress amplitudes on sample EN1410D (A) Applied shear stresses (τ) (B) Measured shear strain (ε) (C) Normal effective stress (σn′) (D) stress path in relation to the peak (p) and residual (r) monotonic failure envelope.

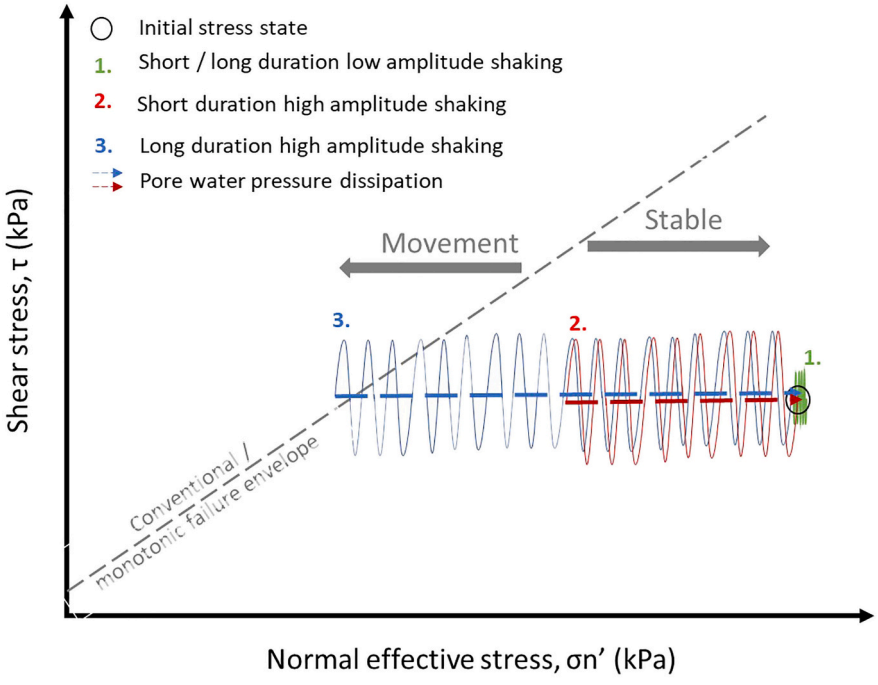

Fig. 12. Conceptual diagram of landslide stress paths during earthquakes of varying duration and ground shaking amplitude.

the normal effective stress remained high, such that the stress path remained below the monotonic failure envelope and no measurable deformation (permanent shear strain) occurred. Thus, low amplitude ground shaking from distant earthquakes, such as that produced by the 2016 Kaikoura earthquake, is unlikely to result in permanent downslope displacement (Table 3).

Whilst excess pore water pressures were generated during short duration dynamic shear experiments conducted at higher shear stress levels, they were not sufficient to reduce the effective normal stress to meet the monotonic failure envelope (Fig. 12, stress path 2). As a consequence, significant shear displacement did not occur. This suggests that earthquakes producing moderate duration, moderate amplitude ground shaking, such as the 2016 Te Araroa earthquake and earthquakes resulting in short duration high magnitude ground shaking such as 2007 Gisborne earthquake, are also unlikely to result in significant landslide movement (Table 3).

During long duration dynamic experiments, in which the imposed shear stresses were comparatively high, permanent displacement did occur (Fig. 11, stress path 3). During these experiments dynamic loading of the sediments generated high pore water pressures that did not result in shear zone liquefaction. Instead shear plane (basal) sliding was initiated once the monotonic failure envelope was reached and was subsequently sustained whilst normal effective stress remains at or above the monotonic failure envelope. This behaviour suggests landslide movement can initiate during earthquakes that generate long duration high amplitude ground shaking, such as local Mw8, subduction zone earthquakes (Table 3). During such events, once the landslide is mobilised the movement would be sustained whilst mean effective stress remains low and would terminate when the ground shaking is no longer sufficient to sustain a very low normal effective stress within the landslide shear zone.

Our results provide a mechanism through which submarine landslides can progressively move and arrest downslope without being subject to catastrophic failure. This mechanism is consistent with interpretations of the failure mode of the TLC based on morphology and subsurface structures (Mountjoy et al., 2009, 2014; Gross et al., 2018; Couvin et al., 2020; Crutchley et al., under review). The results also have broad implications for active margin slope instability since interbedded sandy and silty clay sediments with a high permeability contrast are characteristic sequences on active margins. These bedding relationships can facilitate the rapid development of excess pore water pressures in high permeability sandy beds, meaning that pore pressure cannot dissipate during seismic loading due to overlying fine grained, low permeability material. The development of fluid overpressure in the sediment column has been best studied on passive margins, from direct pore pressure measurements and modelling, and linked to slope instability (Dugan and Sheahan, 2012). Whilst overpressure itself might not be sufficient to trigger slope failure, seismic accelerations from earthquakes can push an intact slope past the point of failure (Stigall and Dugan, 2010). Building on our analysis, if pre-existing excess pore pressure were present in a pre-existing landslide deposit (such as the TLC) prior to earthquake loading, this lower interseismic effective stress condition would increase its sensitivity to movement and arrest during seismic events. This would make the landslide susceptible to more regular episodes of movement during a broader range of earthquake scenarios, however a catastrophic failure with long runout remains unlikely.

This mechanism for long term incremental failure of seafloor slopes is applicable to other margins where coarse grained sediments are delivered at high sedimentation rates to deltas and the continental slope, and where there is the potential for long duration earthquakes (e.g. Cascadia and Nankai Trough). Based on our dynamic loading scenarios and observed displacements, the implications for tsunami hazard from this study are that catastrophic (re)failure and runout of shallow-angled landslide deposits like the TLC are unlikely to occur, even during very large earthquakes, meaning they may represent a low tsunami hazard.

Table 3
Summary of earthquake-induced landslide triggering results.

Earthquake description	Catalogued and expected earthquakes recorded in Gisborne	Laboratory simulation
Long duration low amplitude ground shaking associated with distant high magnitude earthquakes	M7.8 Kaikoura earthquake, 2016	No significant displacement measured
Moderate duration moderate amplitude ground shaking from high magnitude regional earthquakes	M7.1 Te Araroa earthquake, 2016	No significant displacement measured
Short duration high amplitude ground shaking in response to local shallow crustal earthquakes	M 6.7 Gisborne 2004	No significant displacement measured
Long duration high amplitude shaking in response to local subduction earthquakes	MW 8+ Subduction zone earthquakes (simulated)	Significant displacement measured

Our results should be considered in marine geohazard assessments in which landslide scars and deposits are often used as a dataset to determine the potential for future landslide tsunami hazard (Ten Brink et al., 2014). Progressive, low-magnitude failure of a slope can develop a large landslide that may not have any tsunamigenic potential if its mode of failure does not include catastrophic runout.

6. Conclusions

We conducted laboratory experiments in a dynamic back-pressured shearbox on sediments recovered from the base of the Tuaheni Landslide Complex to explore styles of movement under conditions that accurately replicate seismic loading. The seismic loading scenarios we simulated were based on well-characterized historical earthquakes as well as a modelled Mw8 subduction zone earthquake. We found that whilst the sediments are susceptible to liquefaction in certain conditions, liquefaction does not occur at simulated stress states that represent the low angled shear zone in the landslide. Instead, permanent deformation can occur through conventional mobilisation of friction on the shear surface when the sediment's monotonic failure envelope is exceeded. This behaviour occurred during long duration ground shaking simulations where shear stresses were high enough to allow the development of high excess porewater pressures that reduced the normal effective stress sufficiently to mobilise the shear zone. During short and long duration ground shaking simulations, in which shear stresses remained low, the sediments were unable to generate sufficient excess porewater pressures to mobilise the shear surface. This suggests that the landslide is likely to remain stable during most local and regional earthquakes but could be mobilised episodically by long duration high amplitude ground shaking, such as during Mw8 subduction zone earthquakes. Once mobilised the movement would be sustained whilst mean effective stress remains low and would terminate when the ground shaking is no longer sufficient to sustain a very low normal effective stress within the landslide shear zone.

This episodic movement mechanism provides an explanation to why some submarine landslides on active margins display similar morphologies to many known slow-moving terrestrial landslides, and why they may not evolve into catastrophic failures despite being subjected to ground shaking from earthquakes.

Declaration of competing interest

The authors declare that they have no known competing financial interests or personal relationships that could have appeared to influence the work reported in this paper.

Acknowledgements

This research was primarily supported by Marsden Fund Contract NIW1603 and by the NERC/ESRC Increasing Resilience to Natural Hazards programme, grant NE/J01995X/1, NERC/Newton Fund grant NE/N000315, and by MBIE via NIWA SSIF. The officers, crew and scientific teams of SO247 are gratefully thanked for their efforts in acquiring the samples. This research used samples and data provided by the IODP. We thank all staff onboard the *JOIDES Resolution* during Expedition 372 for their support. All IODP drilling data are available from IODP at http://iodp.tamu.edu/scienceops/expeditions/hikurangi_subduction_margin.html. We thank GNS Science staff Dr. Zane Bruce, Giovanni Pradel and Barbara Lyndsell for laboratory support and Dr. Marc-Andrea Brideau for his helpful discussion and suggestions throughout the study.

Appendix A. Supplementary data

Supplementary data to this article can be found online at https://doi.org/10.1016/j.geomorph.2022.108247.

References

Allison, R., Brunsden, D., 1990. Some mudslide movement patterns. Earth Surf. Process. Landf. 15, 297–311.

Barnes, P.M., Pecher, I.A., LeVay, L.J., Bourlange, S.M., Brunet, M.M.Y., Cardona, S., Clennell, M.B., Cook, A.E., Crundwell, M.P., Dugan, B., Elger, J., Gamboa, D., Georgiopoulou, A., Greve, A., Han, S., Heeschen, K.U., Hu, G., Kim, G.Y., Kitajima, H., Koge, H., Li, X., Machado, K.S., McNamara, D.D., Moore, G.F., Mountjoy, J.J., Nole, M.A., Owari, S., Paganoni, M., Petronotis, K.E., Rose, P.S., Screaton, E.J., Shankar, U., Shepherd, C.L., Torres, M.E., Underwood, M.B., Wang, X., Woodhouse, A.D., Wu, H.-Y., 2019a. Site U1517. In: Pecher, I.A., Barnes, P.M., LeVay, L.J., the Expedition 372A Scientists (Eds.), Creeping Gas Hydrate Slides, Proceedings of the International Ocean Discovery Program, 372A. International Ocean Discovery Program, College Station, TX. https://doi.org/10.14379/iodp.proc.372A.103.2019.

Barnes, P.M., Pecher, I.A., LeVay, L.J., Bourlange, S.M., Brunet, M.M.Y., Cardona, S., Clennell, M.B., Cook, A.E., Crundwell, M.P., Dugan, B., Elger, J., Gamboa, D., Georgiopoulou, A., Greve, A., Han, S., Heeschen, K.U., Hu, G., Kim, G.Y., Kitajima, H., Koge, H., Li, X., Machado, K.S., McNamara, D.D., Moore, G.F., Mountjoy, J.J., Nole, M.A., Owari, S., Paganoni, M., Petronotis, K.E., Rose, P.S., Screaton, E.J., Shankar, U., Shepherd, C.L., Torres, M.E., Underwood, M.B., Wang, X., Woodhouse, A.D., Wu, H.-Y., 2019b. Expedition 372A summary. In: Pecher, I.A., Barnes, P.M., LeVay, L.J., the Expedition 372A Scientists (Eds.), Creeping Gas Hydrate Slides, Proceedings of the International Ocean Discovery Program, 372A. International Ocean Discovery Program, College Station, TX. https://doi.org/10.14379/iodp.proc.372A.101.2019.

Bellwald, B., Urlaub, M., Hjelstuen, B.O., Sejrup, H.P., Sørensen, M.B., Forsberg, C.F., Vanneste, M., 2019. NE Atlantic continental slope stability from a numerical modeling perspective. Quat. Sci. Rev. 203, 248–265.

Brain, M.J., Rosser, N.J., Sutton, J., Snelling, K., Tunstall, N., Petley, D.N., 2015. The effects of normal and shear stress wave phasing on coseismic landslide displacement. J. Geophys. Res. Earth Surf. 120, 1009–1022.

Brunet, Morgane, Le Friant, Anne, Boudon, Georges, Lafuerza, Sara, Talling, Peter, Hornbach, Matthew, Ishizuka, Osamu, Lebas, Elodie, Guyard, Hervé, Expedition, I.O. D.P., 340 Science Party., 2016. Composition, geometry, and emplacement dynamics of a large volcanic island landslide offshore Martinique: from volcano flank-collapse to seafloor sediment failure? Geochem. Geophys. Geosys. 17 (3), 699–724.

BSI (British Standard Institute), 1990. British standards methods of test for soils for civil engineering purposes. Part 7: shear strength tests. In: BS 1377: Part 7 (London, United Kingdom).

Bull, S., Cartwright, J., Huuse, M., 2009. A subsurface evacuation model for submarine slope failure. Basin Res. 21, 433–443.

Carey, J.M., McSaveney, M.J., Lyndsell, B.M., Petley, D., 2016. Laboratory simulation of a slow landslide mechanism. In: Aversa, S., et al. (Eds.), Landslides and Engineered Slopes: Experience, Theory and Practice, Proceedings of the 12th International Symposium on Landslides. CRC Press, Boca Raton, Fl, pp. 557–564.

Carey, J.M., Massey, C.I., Lyndsell, B., Petley, D.N., 2019a. Displacement mechanisms of slow-moving landslides in response to changes in porewater pressure and dynamic stress. Earth Surf. Dyn. 7, 707–722.

Carey, J.M., Crutchley, G.J., Mountjoy, J.J., Petley, D.N., McSaveney, M.J., Lyndsell, B., 2019b. Slow episodic movement driven by elevated pore-fluid pressures in shallow subaqueous slopes. Geomorphology 329, 99–107.

Clark, K., Howarth, J., Litchfield, N., Cochran, U., Turnball, J., Dowling, L., Howell, A., Berryman, K., Wolfe, F., 2019. Geological evidence for past large earthquakes and tsunamis along the Hikurangi subduction margin, New Zealand. Mar. Geol. 412, 139–172.

Clarke, J.E.H., 2018. Multibeam echosounders. In: Submarine Geomorphology. Springer, Cham, pp. 25–41.

Collins, B.D., Jibson, R.W., 2015. Assessment of existing and potential landslide hazards resulting from the April 25, 2015 Gorkha, Nepal earthquake sequence. In: U.S. Geological Survey OpenFile Report 2015-1142, Reston, VA.

Couvin, B., Georgiopoulou, Mountjoy, J.J., Lawrence, A., Crutchley, G.G., Brunet, M., Cardona, S., Gross, F., Bottner, C., Krastel, S., Petcher, I., 2020. A new depositional model for the Tuaheni Landslide Complex, Hikurangi Margin, New Zealand. In: Georiopoulou, A., et al. (Eds.), Geological Subaqueous Mass Movements and their Consequences, Advances in Process Understanding, Monitoring and Hazard Assessments Society of Landon Special Publications, 500, pp. 551–566.

Cox, S.C., Menzies, C.D., Sutherland, R., Denys, P.H., Chamberlain, C., Teagle, D.A.H., 2015. Changes in hot spring temperature and hydrogeology of the Alpine Fault hanging wall, New Zealand, induced by distal South Island earthquakes. Geofluids 15 (1–2), 216–239.

Crutchley, G.J., Elger, J., Kuhlmann, J., Mountjoy, J.J., Orpin, A., Georgiopoulou, A., Carey, J., Dugan, B., Cardona, S., Han, S., Cook, A., Screaton, E.J., Pecher, I.A., Barnes, P., Huhn, K., 2022. Investigating the basal shear zone of submarine Tuaheni Landslide Complex, New Zealand: a core-log seismic integration study. J. Geophys. Res. Solid Earth 127 (1), e2021JB021997.

Dugan, B., Flemings, P.B., 2000. Overpressure and fluid flow in the New Jersey continental slope: implications for slope failure and cold seeps. Science 289, 288–291.

Dugan, B., Sheahan, T.C., 2012. Offshore sediment overpressures of passive margins: Mechanisms, measurement, and models. Rev. Geophys. 50 (3), RG3001.

Dyvik, R., Berre, S., Lacasse, S., Raadim, B., 1987. Comparison of truly undrained and constant volume direct simple shear tests. Geotechnique. 37, 3–10.

Field, M.E., Gardner, J.V., Jennings, A.E., Edwards, B.D., 1982. Earthquake-induced sediment failures on a 0.25° slope, Klamath River delta, California. Geology 10 (10), 542–546.

Flemings, P.B., Stump, B.B., Finkbeiner, T., Zoback, M., 2002. Flow focusing in overpressured sandstones: theory, observations and applications. Am. J. Sci. 302 (10), 827–855.

Gross, F., Mountjoy, J.J., Crutchley, G.J., Böttner, C., Koch, S., Bialas, J., Pecher, I., Woelz, S., Dannowski, A., Micallef, A., Huhn, K., Krastel, S., 2018. Free gas distribution and basal shear zone development in a subaqueous landslide – insight from 3D seismic imaging of the Tuaheni Landslide Complex, New Zealand. Earth Planet. Sci. Lett. 502, 231–243.

Hampton, M.A., Lee, H.J., Locat, J., 1996. Submarine landslides. Rev. Geophys. 34, 33–59.

Helmsetter, A., Sornette, D., Grasso, J.R., Anderson, V., Gluzman, S., Pisarenko, V., 2003. Slider-block friction model for landslides: implications for prediction of mountain collapse. J. Geophys. Res. 109 (B02), 210–225.

Holden, C., Kaneko, Y., Anastasio, E.D., Benites, R., Fry, B., Hamling, I., 2017. The 2016 Kaikoura earthquake revealed by kinematic source inversion and seismic wavefield simulations: slow rupture propagation on a geometrically complex crustal fault network. Geophys. Res. Lett. 44 (2), 11,320–11,328.

Howarth, J.D., Orpin, A.R., Kaneko, Y., Strachan, L.J., Nodder, S.D., Mountjoy, J.J., Barnes, P., Bostock, H.C., Holden, C., Jones, K., Cagatay, M.N., 2021. Calibrating the marine turbidite palaeoseismometer using the 2016 Kaikoura earthquake. Nat. Geosci. 14, 161–167.

Huhn, K., 2016. Cruise Report/Fahrtbericht SO247 – SlamZ: Slide Activity on the Hikurangi Margin, New Zealand, Wellington (NZ): 27.03.2016–Auckland (NZ): 27.04.2016. MARUM, Center for Marine Environmental Sciences, Bremen, Germany.

Hühnerbach, V., Masson, D.G., 2004. Landslides in the North Atlantic and its adjacent seas: an analysis of their morphology, setting and behaviour. Mar. Geol. 213 (1–4), 343–362.

Hungr, O., Leroueil, S., Picarelli, L., 2014. The Varnes classification of landslide types, an update. Landslides 11, 167–194.

Kaneko, Y., Ito, Y., Chow, B., Wallace, L.M.M., Tape, C., Grapenthin, R., D'Anastasio, E., Henrys, S., Hino, R., 2019. Ultra-long duration of seismic ground motion arising from a thick, low-velocity sedimentary wedge. J. Geophys. Res. Solid Earth 124, 10347–10359.

Katz, O., Reuven, E., Aharonov, E., 2015. Submarine landslides and fault scarps along the eastern Mediterranean Israeli continental-slope. Mar. Geol. 369, 100–115.

Kelner, M., Migeon, S., Tric, E., Couboulex, F., Dano, A., Lebourg, T., Taboada, A., 2016. Frequency and triggering of small-scale submarine landslides on decadal timescales: analysis of 4D bathymetric data from the continental slope offshore Nice (France). Mar. Geol. 379, 281–297.

Krastel, S., Li, W., Urlaub, M., Georgioupoulou, A., Wynn, R.B., Schwenk, T., Stevenson, C., Feldens, P., 2018. Mass wasting along the NW African continental margin. In: Lintern, D.G., et al. (Eds.), Subaqueous Mass Movements and Their Consequences: Assessing Geohazards, Environmental Implications and Economic Significance of Subaqueous Landslides, Geological Society, London, Special Publications, 477, pp. 151–167.

Kuhlman, J., Orpin, A., Mountjoy, J.J., Crutchley, G., Henrys, S., Lunenburg, R., Huhn, K., 2018. Seismic and lithofacies characterization of a gravity core transect down the submarine Tuaheni Landslide Complex, northeastern New Zealand (SP477) subaqueous mass movements and their consequences. In: Lintern, D.G., et al. (Eds.), Assessing Geohazards, Environmental Implications and Economic Significance of Subaqueous Landslides, Geological Society of London Special Publications, 477, pp. 475–479.

Lay, T., Wallace, T., 1995. Modern Global Seismology. Academic Press, Inc., Cambridge, MA, p. 521.

Lee, H.J., 2009. Timing of occurrence of large submarine landslides on the Atlantic Ocean margin. Mar. Geol. 264 (1–2), 53–64.

Li, G., West, A.J., Densmore, A.L., Jin, Z., Parker, R.N., Hilton, R.G., 2014. Seismic mountain building: Landslides associated with the 2008 Wenchuan earthquake in

the context of a generalized model for earthquake volume balance. Geochem. Geophys. Geosyst. 15, 833–844.
Litchfield, N.J., Van Dissen, R., Sutherland, R., Barnes, P.M., Cox, S.C., Norris, R., Beavan, R.J., Langridge, R., Villamor, P., Berryman, K., Stirling, M., Nicol, A., Nodder, S., Lamarche, G., Barrell, D.J.A., Pettinga, J.R., Little, T., Pondard, N., Mountjoy, J.J., Clark, K., 2014. A model of active faulting in New Zealand. N. Z. J. Geol. Geophys. 57, 32–56.
Locat, J., Lee, H.J., 2002. Submarine landslides: advances and challenges. Can. Geotech. J. 36, 193–212.
Massey, C.I., Petley, D.N., McSaveney, M.J., 2013. Patterns of reactivated landslides. Eng. Geol. 159, 1–19.
Massey, C.I., Townsend, D.B., Rathje, E., Allstadt, K.E., Lukovic, B., Kaneko, Y., Bradley, B., Wartman, J., Jibson, R.W., Petley, D.N., Horspool, N.A., Hamling, I.J., Carey, J.M., Cox, S.C., Davidson, J., Dellow, G.D., Godt, G.W., Holden, C., Jones, K. E., Kaiser, A.E., Little, M., Lyndsell, B.M., McColl, S., Morgenstern, R.M., Rengers, F. K., Rhoades, D.A., Rosser, B.J., Strong, D.T., Singeisen, C., Villeneuve, M., 2018. Landslides triggered by the 14 November 2016 Mw 7.8 Kaikoura earthquake, New Zealand. Bull. Seismol. Soc. Am. 108 (3B), 1630–1648.
Masson, D.G., Harbitz, C.B., Wynn, R.B., Pedersen, G., Løvholt, F., 2006. Submarine landslides: processes, triggers and hazard prediction. Phil. Trans. R. Soc. Am.: Math., Phys. Eng. Sci. 364 (1845), 2009–2039.
Micallef, Aaron, Masson G, Douglas, Berndt, Christian, Stow A.V., Dorrik, 2007. Morphology and mechanics of submarine spreading: A case study from the Storegga Slide. J. Geophys. Res. Earth Surf. 112 https://doi.org/10.1029/2006JF000739, 2007.
Micallef, A., Foglini, F., Le Bas, T., Angeletti, L., Maselli, V., Pasuto, A., Taviani, M., 2013. The submerged paleolandscape of the Maltese Islands, Morphology, evolution and relation to Quaternary change. Mar. Geol. 335, 129–147.
Micallef, A., Mountjoy, J.J., Krastel, S., Crutchley, G., Koch, S., 2016. Shallow gas and the development of a weak layer in submarine spreading, Hikurangi Margin (New Zealand). In: Lamarche, G., et al. (Eds.), Submarine Mass Movements and their Consequences, Advances in Natural and Technological Hazards Research, 41, pp. 419–426.
Motazedian, D., Atkinson, G.M., 2005. Stochastic finite-fault modeling based on a dynamic corner frequency. Bull. Seismol. Soc. Am. 95, 995–1010.
Mountjoy, J.J., Micallef, A., 2018. Submarine landslides. In: Micallef, A., Krastel, S., Savini, A. (Eds.), Submarine Geomorphology, Geological Society of London, Memoirs, pp. 35–250.
Mountjoy, J.J., McKean, J., Barnes, P.M., Pettinga, J.R., 2009. Terrestrial-style slow-moving earthflow kinematics in a submarine landslide complex. Mar. Geol. 267, 114–127.
Mountjoy, J.J., Pecher, I., Henrys, S., Crutchley, G., Barnes, P.M., Plaza-Faverola, A., 2014. Shallow methane hydrate system controls ongoing, downslope sediment transport in a low-velocity active submarine landslide complex, Hikurangi margin, New Zealand. Geochem. Geophys. Geosyst. 15, 4137–4156.
Nadim, F., 2006. Challenges to geo-scientists in risk assessment for submarine slides. Norwegian J. Geol./Norsk Geologisk Forening 86 (3), 351–361.
Pecher, I.A., Barnes, P.M., LeVay, L.J., Expedition 372A Scientists, 2019. Creeping Gas Hydrate Slides: Proceedings of the International Ocean Discovery Program, 372A. International Ocean Discovery Program, College Station, TX.
Petley, D.N., Oven, K., Mitchell, W.A., Rosser, N.J., Dunning, S.A., Allison, R.J., 2006. The role of global and regional precipitation patterns in landslide generation. In: Ashaari, M. (Ed.), Proceedings of the International Conference on Slopes Malaysia 2006. Public Works Department, Kuala Lumpur, pp. 249–268.
Prior, D.B., Coleman, J.M., 1978. Disintegrating retrogressive landslides on very-low-angle subaqueous slopes, Mississippi delta. Marine Geores. Geotechnol. 3 (1), 37–60.
Riboulot, V., Cattaneo, A., Sultan, N., Garziglia, S., Ker, S., Imbert, P., Voisset, M., 2013. Sea-level change and free gas occurrence influencing a submarine landslide and pockmark formation and distribution in deepwater Nigeria. Earth Planet. Sci. Lett. 375, 78–91.
Sassa, K., He, B., Miyagi, T., Strasser, M., Konagai, K., Ostric, M., Setiawan, H., Takara, K., Nagai, O., Yamashiki, Y., Tutumi, S., 2012. A hypothesis of the Senoumi submarine megaslide in Surga Bay in Japan – based on the undrained dynamic loading ring shear tests and computer simulation. Landslides 9, 439–455.
Schumann, K., Stipp, M., Behrmann, J.H., Klaeschen, D., Schulte-Kortnack, D., 2014. P and S wave velocity measurements of water-rich sediments from the Nankai Trough, Japan. J. Geophys. Res. Solid Earth. 119, 787–805.
Screaton, E.J., Torres, M.E., Dugan, B., Heeschen, K.U., Mountjoy, J.J., Ayres, C., Rose, P. S., Pecher, I.A., Barnes, P.A., LeVay, L.J., 2019. Sedimentation controls on methane-hydrate dynamics across glacial/interglacial stages: an example from International Ocean Discovery Program Site U1517, Hikurangi Margin. Geochem. Geophys. Geosyst. 20, 4906–4921.
Singh, S.K., Mena, E., Castro, R., 1988. Some aspects of source characteristics of the 19 September 1985 Michoacan earthquake and ground motion amplification in the near Mexico City from strong motion data. Bull. Seismol. Soc. Am. 78 (2), 451–477.
Stigall, J., Dugan, B., 2010. Overpressure and earthquake initiated slope failure in the Ursa region, northern Gulf of Mexico. J. Geophys. Res. 115, B04101.
Stirling, M., 2012. A New Seismic hazard model for New Zealand. Bull. Seismol. Soc. Am. 92 (5), 1878–1903.
Talling, P.J., Wynn, R.B., Masson, D.G., Frenz, M., Cronin, B.T., Schiebel, R., Akhmetzhanov, A.M., Dallmeier-Tiessen, S., Benetti, S., Weaver, P.P.E., Georgiopoulou, A., Zühlsdorff, C., Amy, L.A., 2007. Onset of submarine debris flow deposition far from original giant landslide. Nature 450 (7169), 541–544.
Ten Brink, U.S., Chaytor, J.D., Geist, E.L., Brothers, D.S., Andrews, B.D., 2014. Assessment of tsunami hazard to the US Atlantic margin. Mar. Geol. 353, 31–54.
Urlaub, M., Talling, P.J., Masson, D., 2015. What causes large submarine landslides on low gradiens (<2°) continental slopes with slow (~0.15 m/Kyr) sediment accumulation? J. Geophys. Res., Soild Earth. 120, 6722–6739.
Valagussa, A., Frattini, P., Crosta, G.B., Valbuzzi, E., 2016. Pre and post Nepal earthquake landslide inventories. In: Aversa, S., Cascini, L., Picarelli, L., Scavia, C. (Eds.), Landslides and Engineered Slopes: Experience, Theory and Practice: Proceedings of the 12th International Symposium on Landslides, pp. 1957–1964. Boca Raton, Fla.
Viesca, R.C., Rice, J.R., 2012. Nucleation of slip-weakening rupture instability in landslides by localized increase of pore pressure. J. Geophys. Res. 117, B03104.
Wallace, L.M., Beavan, J., 2010. Diverse slow slip behavior at the Hikurangi subduction 390 margin, New Zealand. J. Geophys. Res. 115, B007717.
Wallace, L.M., Beavan, J., Bannister, S., Williams, C., 2012. Simultaneous long-term and short-term slow slip events at the Hikurangi subduction margin, New Zealand: implications for processes that control slow slip event occurrence, duration, and migration. J. Geophys. Res. 112, B009489.
Watson, S.J., Mountjoy, J.J., Crutchley, G.J., 2020. Tectonic and geomorphic controls on the distribution of submarine landslides across active and passive margins, eastern New Zealand. In: Georgiopoulou, A., et al. (Eds.), Subaqueous Mass Movement and Their Consequences, Advances in process Understanding, Monitoring and Hazard Assessments, 500, pp. 447–494.